J Neurophysiol
88: 2700–2712, 2002; 10.1152/jn.00237.2002.

Conditions for the Triggering of Spreading Depression Studied With Computer Simulations

H. KAGER,[1] W. J. WADMAN,[1] AND G. G. SOMJEN[2]
[1]*Swammerdam Institute for Life Sciences, Section Neurobiology, University of Amsterdam, 1098 SM Amsterdam, The Netherlands; and* [2]*Department of Cell Biology, Duke University Medical Center, Durham, North Carolina 27710*

Received 1 April 2002; accepted in final form 24 July 2002

Kager, H., W. J. Wadman, and G. G. Somjen. Conditions for the triggering of spreading depression studied with computer simulations. *J Neurophysiol* 88: 2700–2712, 2002; 10.1152/jn.00237.2002. In spite of five decades of study, the biophysics of spreading depression (SD) is incompletely understood. Earlier we have modeled seizures and SD, and we have shown that currents through ion channels normally present in neuron membranes can generate SD-like depolarization. In the present study, we define the conditions for triggering SD and the parameters that influence its course in a model of a hippocampal pyramidal cell with more complete representation of ions and channels than the previous version. "Leak" conductances for Na^+, K^+, and Cl^- and an ion pump were present in the membrane of the entire cell; fast inactivating voltage dependent conductances for sodium and potassium in the soma; "persistent" conductances in soma and apical dendrite, and K^+- and voltage-dependent *N*-methyl-D-aspartate (NMDA)-controlled conductance in the apical dendrite. The neuron was surrounded by restricted interstitial space and by a "glia-endothelium" system of extracellular ion regulation bounded by a membrane having leak conductances and an ion pump. Ion fluxes and concentration changes were continuously computed as well as osmotic cell volume changes. As long as reuptake into the neuron and "buffering" by glia kept pace with K^+ released from the neuron, stimulating current applied to the soma evoked repetitive firing that stopped when stimulation ceased. When glial uptake was reduced, K^+ released from neurons could accumulate in the interstitium and keep the neuron depolarized so that strong depolarizing pulses injected into the soma were followed either by afterdischarge or SD. SD-like depolarization was ignited when depolarization spreading into the apical dendrite, activated persistent Na^+ current and NMDA-controlled current. With membrane parameters constant, varying the injected stimulating current influenced SD onset but neither the depolarization nor the increase in extracellular K^+. Glial "leak" conductance influenced SD duration and SD ignition point. Varying maximal conductances (representing channel density) also influenced SD onset time but not the amplitude of the depolarization. Hypoxia was simulated by turning off the Na-K exchange pump, and this resulted in SD-like depolarization. The results confirm that, once ignited, SD runs an all-or-none trajectory, the level of depolarization is governed by feedback involving ion shifts and glutamate acting on ion channels and not by the number of channels open, and SD is ignited if the net persistent membrane current in the apical dendrites turns inward.

INTRODUCTION

Spreading depression (SD) of Leão (Bureš et al. 1974; Leão 1944) is characterized by massive depolarization of neurons associated with redistribution of ions across cell membranes. In spite of more than five decades of study, the biophysical mechanism of the depolarization is incompletely understood. The trajectory of the membrane potential (V_m) suggests a regenerative, all-or-none type process governed by positive feedback. The earliest explanation of SD postulating feedback was Grafstein's potassium hypothesis (Grafstein 1956). Grafstein suggested that K^+ ions released from neurons during the firing of action potentials could accumulate in the limited interstitial space of the CNS. If excessive firing elevated extracellular K^+ concentration sufficiently, it could further depolarize the neurons that released them until inactivation silenced the firing. Grafstein's hypothesis seemed refuted when it turned out that tetrodotoxin (TTX), which prevents action potential firing, did not block SD (García Ramos and de la Cerda 1974; Tobiasz and Nicholson 1982). Since then it has become clear, however, that K^+ can be released from neurons without the firing of impulses. An alternative hypothesis proposed by van Harreveld, attributed to glutamate the role assigned by Grafstein to K^+ (van Harreveld 1959; van Harreveld and Fifková 1970). van Harreveld later suggested that there are two kinds of SD, one mediated by K^+ and the other by glutamate (van Harreveld 1978).

Identifying the agents that mediate SD solves only part of the problem. The other major question concerns the mechanism of the massive transmembrane flux of ions causing the depolarization. Considered broadly, these membrane changes could result from the abnormal operation of physiological ion channels or from the opening of pathological pathways not normally present in the membrane. Pharmacological blockade of certain physiological channels can postpone SD and the related hypoxic SD-like depolarization (HSD) without reliably suppressing them (for recent review, see (Somjen 2001). Simultaneous blockade of all known major inward currents does, however, effectively prevent HSD, suggesting that the depolarization is the result of cooperative action of several physiological channels (Müller and Somjen 1998; Somjen 2001). Our recent computer simulations supported the idea that there can be more than one agent inducing SD and also that ion channels known to exist in the membrane of cerebral neurons can provide the pathway for the ion fluxes that generate the depolarization (Kager et al. 2000). Using the "Neuron" simu-

Address for reprint requests: G. Somjen, Dept. of Cell Biology, Box 3011, Duke University Medical Center, Durham, NC 27710, (E-mail: g.somjen@cellbio.duke.edu).

The costs of publication of this article were defrayed in part by the payment of page charges. The article must therefore be hereby marked "*advertisement*" in accordance with 18 U.S.C. Section 1734 solely to indicate this fact.

lation environment of Hines, Moore, and Carnevale (Hines and Carnevale 1997) we have shown that either a membrane ion current modeled after the persistent sodium current ($I_{Na,P}$), or one controlled by NMDA receptors (I_{NMDA}) can generate SD-like depolarization, and when both conductances are available, the depolarization has a lower threshold, it starts earlier, and it lasts longer than when either acts alone (Kager et al. 2000).

The purpose of the present series of simulated trials was to define the conditions for the initiation of SD and to assess the relative influence of various membrane parameters on its course. In the previous version of the model (Kager et al. 2000), Na^+ and K^+ were the only ions represented. We have now added Cl^- and impermeant intracellular anions (A^-) to the list so that electro-neutrality of solutions could be preserved and osmotically induced cell volume changes computed. Adjustable "leak" conductances for the three permeant ions and "active" conductances for Na^+ and K^+ were inserted into the neuron membrane. Unlike the previous version, the glia-endothelial "ion-buffer" system was simulated by a membrane-bound "compartment" in contact with the interstitial space. The "resting" volume of the glial compartment and the leak conductances of its membrane were adjustable. As before, the neuron was surrounded by a limited interstitial space. Unlike in the previous version, osmotic imbalance caused changes in the volume of the neuron and the glial cell, and the interstitial volume fraction (ISVF) varied inversely with the cell volumes. Diffusion of ions along the interstitial space and among the parts of the neuron and the glial compartment was also computed.

The simulations confirmed that an uncontrolled rise of extracellular potassium concentration ($[K^+]_o$) and of spilled glutamate can cooperate in the generation of SD. SD was ignited when depolarization of apical dendrites and the rise of extracellular K^+ concentration ($[K^+]_o$) activated persistent inward currents ($I_{Na,P}$ and/or I_{NMDA}) in the dendritic membranes sufficiently so that these exceeded the summed outward currents, and as a result, the net (total) membrane current turned inward. Changes in glial leak conductance, which determined glial buffering power, powerfully influenced the ability to generate SD.

Some of the results have been published in abstracts (Kager et al. 2001; Somjen et al. 2001) and are briefly mentioned in two reviews (Somjen 2001, 2002).

METHODS

All simulations were executed in the Neuron modeling environment by Hines, Moore and Carnevale (Hines and Carnevale 1997). We used Neuron version 5.0 in which longitudinal diffusion of ions is incorporated.

Morphology

We used two models with different morphologies for our simulations. A "simplified" cell consisting of a soma with unbranched basal and apical dendrites attached and a "complete" cell, reconstructed from a rat CA1 pyramidal cell from the Duke-Southampton Archive of Neuronal Morphology (Cannon et al. 1998). The neuron was subdivided into segments that are units for computations. They do not have a unique morphological counterpart; several segments may be used to design a morphological relevant segment of a neuron, such as a soma or a dendritic shaft. The apical dendrite of the simplified cell had six segments (labeled D0 –D5) subdivided into 14 subsegments. The basal dendrite and the soma consisted of single segments, the soma with three subsegments and the basal dendrite with four subsegments. The soma tapered from 10 to 6 μm diameter with a length of 30 μm. The basal dendrite was a cylinder of 3 μm diam and 100 μm length. The apical dendritic segments decreased in diameter from 4 to 1 μm, with a length of 400 μm for segments D0–D4, and 200 μm for D5. The somatic region of the complete cell consisted of four segments with attached a branched apical dendritic tree of 45 segments and a branched basal dendritic tree of 52 segments. The segments were subdivided into subsegments to assure that no computational unit exceeded 0.1 electrotonic lengths. An image of the complete cell appeared in our previous report (Kager et al. 2000). We defined several regions for the simple cell and mapped this to the complete cell so that comparable regions possessed similar biophysical properties. All illustrated recordings were from the center of a segment.

The electrotonic distance from soma to the tip of the apical dendrite was between 1 and 3 length constants for the simplified cell. The leakage conductances of the simplified cell were adjusted to yield an input resistance comparable to that of the complete cell (between 50 and 80 MΩ in different simulations, see following text). The electrotonic length of the complete cell was slightly larger than that of the simplified cell.

Each neuronal segment communicated with a segment of the interstitial space, which was in turn connected to a glial segment. Each segment is defined by a volume and by the cross section of the membrane that connects it to a segment of a different type (neuron to interstitial space and interstitial space to glia); this membrane contains ion channels and ion pumps. Segments of the same type can be connected through a cross section that permits unrestricted diffusion of ions. The volume of the interstitial space and of the glial segments are deduced from the volume of the neuronal segment that they surround (see Table 1). We did not calculate the extracellular field generated by the single neuron, effectively setting the extracellular resistance to zero.

A complete simulation with the complete cell lasted many hours. For this reason most of the data requiring systematic changes in parameters were carried out with the simplified cell. This report is based on 68 simulations with the simplified cell and 12 simulations with the complete cell.

Passive electrical properties

The membranes that separated the neuronal and the glial compartments from the interstitium contained permeabilities for sodium, potassium, and chloride ions. The ion specific currents were calcu-

TABLE 1. *Initial ("resting") conditions*

	Neuron	Interstitial Fluid	Glial Compartment
Membrane potential, mV	−69.1	0	−87.7
Na^+ concentration, mM	10	140	30
K^+ concentration, mM	133.5	3.5	113.5
Cl^- concentration, mM	10.4	143.5	4.8
Impermeant anion (A^-), mM	133.1	0	138.7
Relative volume*	1.0	0.15	10.0

* The glial compartment was adjusted to different volumes in some simulations (see text).

lated according to the Goldman-Hodgkin-Katz (GHK) current equation

$$I_{GHK}(t) = P_{ion} * V_m * z\alpha F * \frac{[ion]_i - [ion]_o e^{-\alpha V}}{1 - e^{-\alpha V}} \text{ with } \alpha = \frac{zF}{RT}$$

where I_{GHK} is in mA/cm^2, P_{ion} is the membrane permeability for *ion* in cm/s, as defined by Hines and Carnevale (Hines and Carnevale 1997), F is Faraday's constant, R is the gas constant, T is the absolute temperature, z the valence of *ion*, and where $[ion]_i$, $[ion]_o$, and V_m are functions of time.

The density of leak permeabilities in the membrane determined the value of the input resistance R_i of the neuron, which was normally between 50 and 80 MΩ for both the simplified and the complete cell. The ratio of permeabilities for potassium and sodium (P_K/P_{Na}) was chosen so that at resting conditions the ratio of leak currents for these two ions $I_{K,leak}/I_{Na,leak}$ was two-thirds (complemented by the 3Na/2K pump). The permeability ratio was $P_K/P_{Na} = 14$. The specific membrane capacitance C_m was 1 μF/cm^2. The neuronal segments were electrotonically coupled with a specific axial resistance R_a of 100 Ωcm. The significant currents were carried by K^+ and Na^+. The permeability for chloride was small in comparison to P_K; it allowed redistribution of chloride ions, but hardly contributed electrically. "Impermeant" anions (A^-) were included for electroneutrality (see following text).

Electroneutrality

The small number of sodium and potassium ions that permeated the membrane under resting conditions were counterbalanced by a Na/K pump so that at the steady-state situation at rest there was no net flux of ions. As Cl^- was the only extracellular anion in our simulations, its initial extracellular concentration ($[Cl^-]_o$) was determined by the sum of both cations: $[Cl^-]_o = [Na^+]_o + [K^+]_o$. We chose intracellular concentration of chloride ($[Cl^-]_i$) to make the Cl^- reversal potential E_{Cl} equal to the resting membrane potential, and therefore there was no need for a Cl^- pump. $[A^-]_i$ was then chosen to make the intracellular subsegments electroneutral: $[A^-]_i = [Na^+]_i + [K^+]_i - [Cl^-]_i$.

Active conductances and their distribution

Voltage-dependent permeabilities were simulated according to Hodgkin and Huxley's kinetic description. The expressions used for the voltage-dependent rate constants were derived from a model of hippocampal CA3 neurons by Traub and colleagues (1994). *N*-methyl-D-aspartate (NMDA)-controlled current was jointly controlled by voltage (imitating Mg^{2+}-dependent gating) and $[K^+]_o$. The distribution of ions was regulated by electrogenic ion pumps transporting 3 Na^+ outward against 2 K^+ inward. The pump activity was stimulated by elevations of $[K^+]_o$ and $[Na^+]_i$. The equations governing the active permeabilities and the ion pump have been reported previously (Kager et al. 2000; Traub et al. 1993).

All membranes contained leak conductances and the 3Na/2K ion pump. The active currents were spatially distributed as follows: transient Na and K currents $I_{Na,T}$ and $I_{K,A}$ were usually present in the somatic membrane only, the persistent Na current $I_{Na,P}$ and the delayed rectifier K current, $I_{K,DR}$, in the soma and in the proximal four of the six apical dendritic segments (D0–D3), and I_{NMDA} in the apical dendrite segments D1–D3. Transient currents $I_{Na,T}$ and I_K were inserted in dendritic segments D0-D3 for a few simulations. The basal dendrite and the most distal two apical dendritic segments (D4 and D5) only contained leak and no voltage-dependent conductances.

Properties of the "glia-endothelial" compartment

The membrane of the "glia-endothelial" compartment contained the same passive components as the neurons (K^+, Na^+, and Cl^- "leak" conductance, 3Na/2K ion pump). The initial glial ion concentrations (K^+, Na^+, Cl^-, and A^-) are shown in Table 1; electroneutrality in the initial condition was generated as described for the neuronal compartment. The ion permeability ratio was about $P_K/P_{Na} = 128$, which is larger than that of the neuronal membrane. The relatively larger P_K in the glial membrane pulled the V_{rest} to only 5 mV depolarized relative to the potassium reversal potential $E_{K,glia}$.

The membrane permeability determined the glial "buffer strength" and was adjusted for various simulations. Unlike adjacent neuronal segments, glial segments were not electrotonically coupled. Ion diffusion between segments was implemented, but due to the large relative volume of the glia (10 times the neuronal volume, except when otherwise indicated), changes in ion concentrations were minute and never lead to a concentration gradient that could drive a significant intra-glial ion flux.

Ion accumulation

An essential feature of the model is that ion concentrations varied over time, continuously affecting the driving force for the currents that the ion carries. Two components contributed: first, ion specific transmembrane fluxes and second, diffusion between connected segments. We distinguished three classes of segments: neuronal, interstitial, and glial compartments. Within each subsegment we assumed instantaneous diffusion equilibrium and thus a single value for [ion]. This value can change as a consequence of specific ion currents through the membrane and due to diffusion from one compartment into another. The first change is described as

$$\frac{d[ion]_i}{dt} = \frac{I_{\Sigma(ion)}}{F * vol^i}$$

where $I_{\Sigma(ion)}$ is the net ion specific transmembrane flux, F is Faraday's constant, and vol^i is the volume of the segment under consideration. Ion fluxes between segments were implemented as driven by concentration differences between neighboring segments. The equation implemented in the Neuron simulation environment was used

$$\frac{d[ion]_i}{dt} = \sum_n D * Surface_{n->i} * \frac{d[ion]}{dx}$$

where $[ion]_i$ is the "ion " concentration in segment i, D is the diffusion constant, assumed equal for all ions, including A^-. The surface $_{n->i}$ is the connecting surface with neighboring segment i to which our segment has a concentration gradient of (d[ion])/(dx).

Osmotic forces

Changes in ion concentrations imply changes in osmolarity in the interstitial space, neuron, and glia compartments. Differences in osmotic value induce changes in volume in these compartments due to water flow from one to the other. Because neurons resist swelling more than other cells (Aitken et al. 1998) and because of the constraints presented in live tissue by neighboring cell elements, the model cell was not allowed to expand beyond the limits imposed by the interstitial volume. We implemented this in a phenomenological way assuming conservation of the total volume. The osmotic pressure in a given compartment ($\pi_{compartment}$) is assumed proportional to the sum of n ions present in that compartment

$$\pi_{compartment} = c * \sum_n [ion]^n_{compartment}$$

The volume of the interstitial space, vol^{is}, is defined as a fraction (0.15, see Table 1) of the initial volume of the neuron (vol_0^{neuron}) that it surrounds, while the glia-endothelial compartment vol^{glia} is assumed to be substantially larger (10, see Table 1) than the neuronal compartment to operate as a potassium buffer. The change in vol^{is} is

related to the difference in osmotic value with both compartments to which it is connected

$$\mathrm{vol}^{\mathrm{is}} = \mathrm{vol}_0^{\mathrm{neuron}} * \left(0.04 + 0.055 * \left[\exp\left(\frac{\pi_{\mathrm{is}} - \pi_{\mathrm{neuron}}}{20} \right) + \exp\left(\frac{\pi_{\mathrm{is}} - \pi_{\mathrm{glia}}}{20} \right) \right] \right)$$

In this way the volume of the interstitial space is 15% of the neuronal volume in the absence of osmotic differences and it can shrink to 4% when pressure builds up, corresponding to values measured during SD and HSD of hippocampal tissue slices (Jing et al. 1994). Conservation of volume dictates that the volume of the neuronal respectively glial compartments are given by

$$\mathrm{vol}^{\mathrm{neuron}} = \mathrm{vol}_0^{\mathrm{neuron}} * \left(1.055 - 0.055 * \exp\left(\frac{\pi_{\mathrm{is}} - \pi_{\mathrm{neuron}}}{20} \right) \right)$$

and

$$\mathrm{vol}^{\mathrm{glia}} = \mathrm{vol}_0^{\mathrm{neuron}} * \left(10.055 - 0.055 * \exp\left(\frac{\pi_{\mathrm{is}} - \pi_{\mathrm{glia}}}{20} \right) \right)$$

From these functions, it is clear that most variation is to be expected to occur in the interstitial space (reduction to maximally 30% of the initial volume) and that the changes in the glial compartment are less than 1%. We assume that changes in volume take time to develop and therefore implemented them as a first-order process with a time constant of 250 ms. In the model, volume is treated as a time-dependent variable, and increasing it will dilute ion concentrations and reduce the osmotic pressure in a compartment.

Calculated variables

The following variables were continuously computed for each segment: membrane currents, ion fluxes; membrane voltage; ion concentrations; ion equilibrium potentials; volume.

RESULTS

As in live neurons, depolarizing current of moderate intensity injected into the soma of the model neuron evoked regularly repeated firing of action potentials, which stopped when current injection was terminated. The key to this normal stability of function was the effective regulation of $[K^+]_o$ by the neuron's Na-K ion pump and the glia-endothelial system. When the regulation of $[K^+]_o$ fell short, seizure- or SD-like behavior resulted. Self-sustained afterdischarges resembling tonic seizures are the topic of a separate study (Kager et al. 2001).

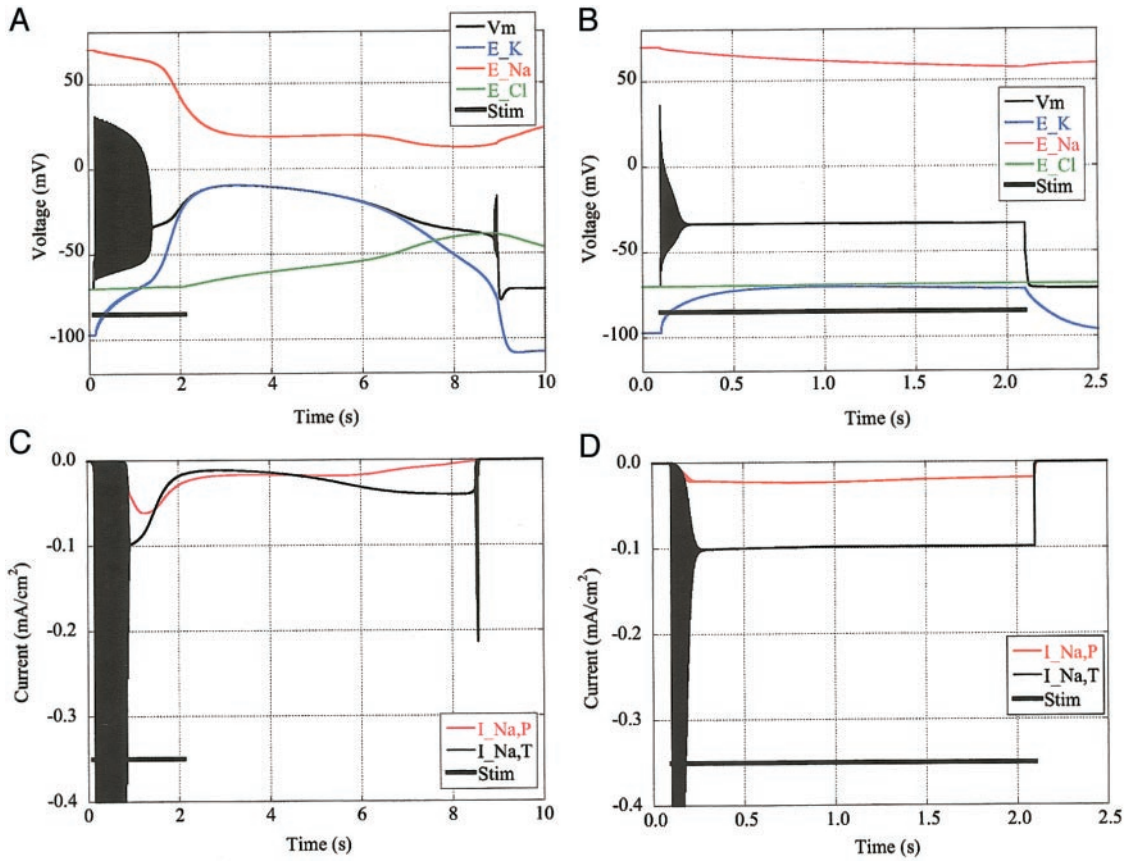

FIG. 1. Triggering simulated spreading depression (SD), and its prevention by increased glial buffering. *A* and *C*: SD in one simulation; *B* and *D*: its absence in another simulation. Note different time scales. *A*: voltages in neuron soma during SD. V_m: membrane potential; *E*_K: equilibrium potential for potassium; *E*_Na: equilibrium potential for sodium; *E*_Cl: equilibrium for chloride; Stim.: time of stimulation. Stimulus strength 0.3 nA for 2 s. *B*: membrane parameters similar to *A*, except that glial leak conductance and ion pump turnover were 4 times higher. The stronger stimulus (0.75 nA for 2 s) did not provoke SD. *C*: soma Na^+ currents during the event represented in *A*. *I*_Na, P: persistent Na^+ current; *I*_Na, T: transient (Hodgkin-Huxley style) Na^+ current; Note small $I_{Na,\,T}$ continuing after cessation of impulse firing, representing the "window" current. *D*: soma Na^+ currents during same simulation as in *B*. Note large window current.

Condition for SD ignition

Figure 1 compares two simulations, differing only in the efficiency of the glia-endothelial "buffer" and stimulus intensity. In the simulation illustrated in Fig. 1, *A* and *C*, a stimulating current injected into the neuron soma caused SD-like depolarization, but in *B* and *D*, an even stronger stimulus failed to evoke SD. The powerful depolarization caused by the stimulus in the case of Fig. 1, *B* and *D*, inactivated and suppressed impulse firing, nevertheless the membrane potential returned to the resting level immediately after cessation of the injected current.

There was no fixed threshold for SD in terms of the stimulus intensity, the increase of $[K^+]_o$, or V_m, but rather a number of factors had to cooperate for SD initiation. For this reason we prefer the term "ignition point" over "threshold." That depolarization is not sufficient, is obvious from comparing two trials represented in Fig. 1, *A* and *C*, and *B* and *D*. The key difference between the two conditions was in the glial leak conductance and the glial $I_{Na\text{-}Kpump}$, which were adjusted to four times higher for *B* and *D* than for *A* and *C*. The stimulus intensity was 0.75 nA in *B* and *D* but only 0.3 nA for *A* and *C*. All other parameters, including the neuronal pump current, were identical in the two trials.

The key event igniting SD took place in the "active" segments of the apical dendrites. This is not apparent in Fig. 1 but is illustrated in Fig. 2. The regenerative SD-like depolarization was ignited if and only if the net (composite) dendritic membrane current turned inward (Figs. 2, *C* and *D*, 4, *A–C*, and 6*B*). A positive feedback cycle was initiated as the sustained net inward current caused continuing depolarization, in turn forcing the release of more K^+ from the dendrite, which in its turn lead to more depolarization (Fig. 3). The critical role of the dendritic sustained inward current for SD ignition is apparent from the expanded tracings in Figs. 2*D* and 4*A*. The net (aggregate) current flowed at first outward in the apical dendrites but then turned sharply inward. In the soma, it was inward when the firing ceased, then it diminished and then briefly turned outward. Thus it was the depolarization of the soma that prepared the ground, but it was in the D1 dendrite segment that the SD-like response was initiated. The trajectories of V_m, pump current, ISVF and $[K^+]_o$ in soma and dendrites shown in Fig. 5 also illustrate that, even though the neuron soma is initially more affected, the dendrites take the lead in actually starting SD. During stimulation, especially while the firing of action potentials continued, the soma was swelling and $[K^+]_o$ around it was rising faster than in the

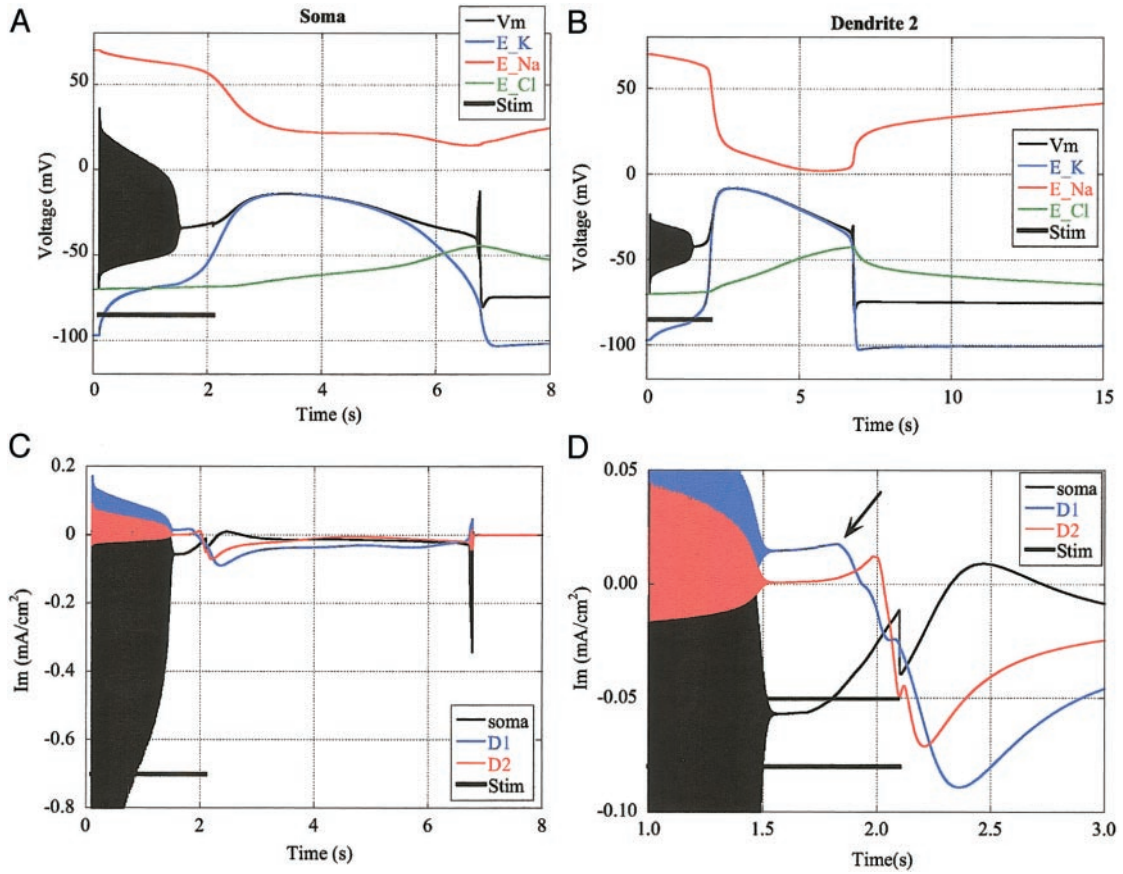

FIG. 2. Membrane voltages and currents in neuron soma and apical dendrite during SD. All 4 panels show data from the same simulation. *A*: voltages in neuron soma. Symbols similar to Fig. 1*A*. Note that E_{Na} continues to decrease while V_m and E_K are gradually recovering, E_K somewhat faster than the depolarized V_m. E_{Cl} begins to shift in the positive direction as Cl^- ions are dragged inward by the inflow of Na^+ when it exceeds the outflow of K^+. *B*: voltages in apical dendritic segment D2. *C*: net (aggregate) membrane currents in the neuron soma and in dendritic segments D1 and D2. Note that the transitional segment D0, which contained $I_{Na,\,P}$ but no I_{NMDA} (see METHODS), is not shown. *D*: the same currents as *C* shown on expanded scales. The oblique arrow marks the inward turn of the net current in the D1 segment. The sudden downshift of the soma I_m at the termination of the stimulus resulted from the abrupt cessation of the stimulating current. The stimulus was 0.385 nA for 2 s.

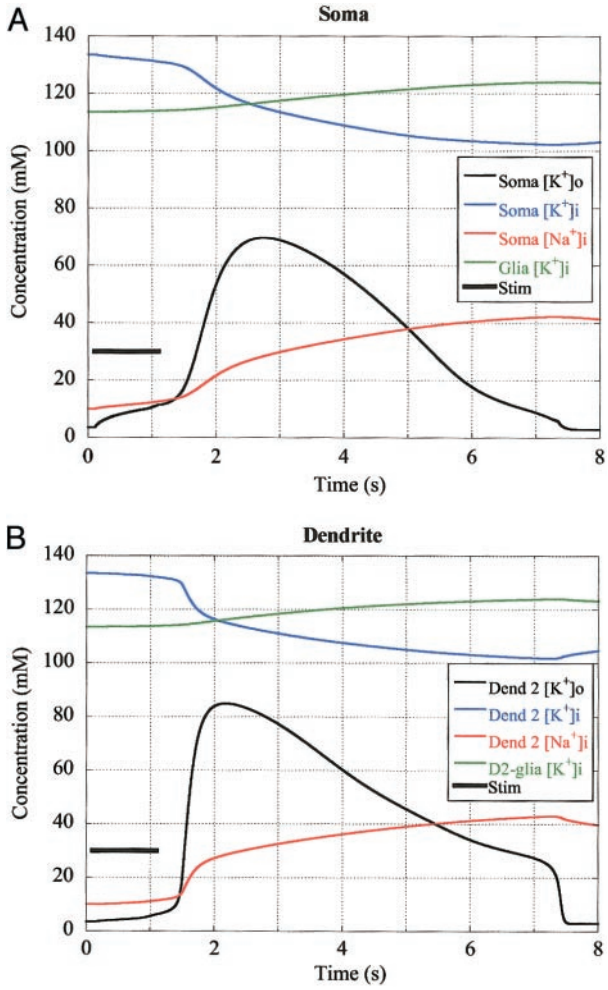

FIG. 3. Ion concentration changes in neuron soma (*A*), 2nd apical dendritic segment (*B*) and adjacent glial compartments during SD. $[K^+]_o$: potassium concentration in interstitial space. Soma $[K^+]_i$: potassium concentration in neuron cytosol. Glia, $[K^+]_i$: potassium concentration in glia cytosol. Soma $[Na^+]_i$: sodium concentration in neuron cytosol. The stimulus was 0.35 nA for 1 s.

region of the dendrites, but SD onset was marked by the abrupt acceleration of swelling and $\Delta[K^+]_o$ in the proximal apical dendrites (Fig. 5, *C* and *D*).

In most of the simulations, the dendritic membranes contained no transient currents ($I_{Na,T}$ and $I_{K,A}$) (see METHODS). Because, however, transient conductances do exist in apical dendrites of CA1 pyramidal neurons (Magee and Johnston 1995), the effect of their presence was tested. Inserting $I_{Na,T}$ and $I_{K,A}$ into the dendritic segments D0–D3 lowered the ignition point for SD and prolonged the duration of the depolarization but did not otherwise change the sequence of events. This is as expected because these transient conductances are inactivated by the profound sustained depolarization. In these trials, the channel density represented by $g_{Na,T}$ in the dendrites remained low and spikes were not initiated in the dendrites.

Evolution of simulated SD

Whenever a stimulating current was strong enough so that the accelerating rise of $[K^+]_o$ progressively depolarized the neuron, the transient sodium conductance ($g_{Na,T}$) began to be inactivated, spikes lost amplitude, and eventually firing ceased (Fig. 1*A*). Yet Na^+ ions continued to trickle into the soma, in part through the persistent Na^+ conductance ($g_{Na,P}$) and also by way of the so called "window" current of $I_{Na,T}$ (Fig. 1*C*). Moreover the depolarization kept $g_{K,DR}$ open allowing K^+ to continue to escape from the neuron. A window current exists in the voltage range where activation begins yet steady-state inactivation is incomplete (i.e., the curves of activation and inactivation overlap) (Ketelaars et al. 2001; Steinhäuser et al. 1990). Depolarization of the soma forced the dendrites to depolarize also (Fig. 2*B*), mediated in part by "passive" current flow (electrotonus) and in part by the diffusion of excess K^+ in the interstitium (Fig. 3*B*). In the apical dendrite segments 1–3 the depolarization activated voltage-controlled currents ($I_{K,DR}$ and $I_{Na,P}$) as well as the NMDA receptor, which is jointly controlled by $[K^+]_o$ and V_m (Fig. 4, *B* and *C*) (see Kager et al. 2000). As the inward currents ($I_{Na} + I_{NMDA}$) began to exceed the outward currents ($I_K + I_{Cl} + I_{Na\text{-}Kpump}$), the net membrane current (I_m) turned inward the apical dendrites (Figs. 2, *C* and *D*, 4, *A–C*, and 6*B*), except the distal apical segments D5 and D6 and the basal dendrites that had only leak conductance. In these passive segments, the net current remained outward (Fig. 4*A*), supplying the "sources" of the current that was flowing through the interstitial space and into the "sinks" generated by the inward current in proximal apical dendritic segments. This conforms to current source densities recorded in live hippocampus of intact rat brains (Wadman et al. 1992).

During SD, $[K^+]_o$ reached a summit and then began to subside even though K^+ ions continued to leave the neuron as indicated by the progressive decrease in $[K^+]_i$ (Fig. 3). It was uptake of K^+ into the glia-endothelial "compartment" plus diffusion in the interstitial space from around the active toward the passive segments that caused $[K^+]_o$ to subside in the face of unabated K^+ release (Figs. 3 and 4*D*). It is important to note that throughout the SD episode there remained a reduced but still substantial gradient between $[K^+]_i$ and $[K^+]_o$, as it is in live tissue (Müller and Somjen 2000a). At the height of the depolarization, V_m was dominated by E_K (Figs. 1*A* and 2, *A* and *B*). In this depolarized state membrane currents were much reduced (Figs. 2*C* and 4) because the driving force propelling ions became small and also because of the closure of inactivating channels.

In the example shown in Fig. 5*A*, there were brief bursts of truncated (partially inactivated) action potentials after cessation of stimulation as well as at the start of repolarization. This was seen in some but not all simulations, determined by the rates of the removal of inactivation and of repolarization.

Effect of varying parameters on the SD process

Similarly to action potentials, SD was an all-or-none event. The magnitude and trajectory of the depolarization and of the membrane currents were independent of the stimulus, provided that the stimulus intensity remained above the ignition point and membrane parameters were kept constant. The strength of the stimulating current did, however, influence the onset time of the SD (Fig. 6). As a further analogy to action potentials, there appeared to be a strength-duration requirement to igniting SD. Reducing stimulus pulse duration from 1,000 to 500 ms had little effect on the SD ignition point, but further shortening

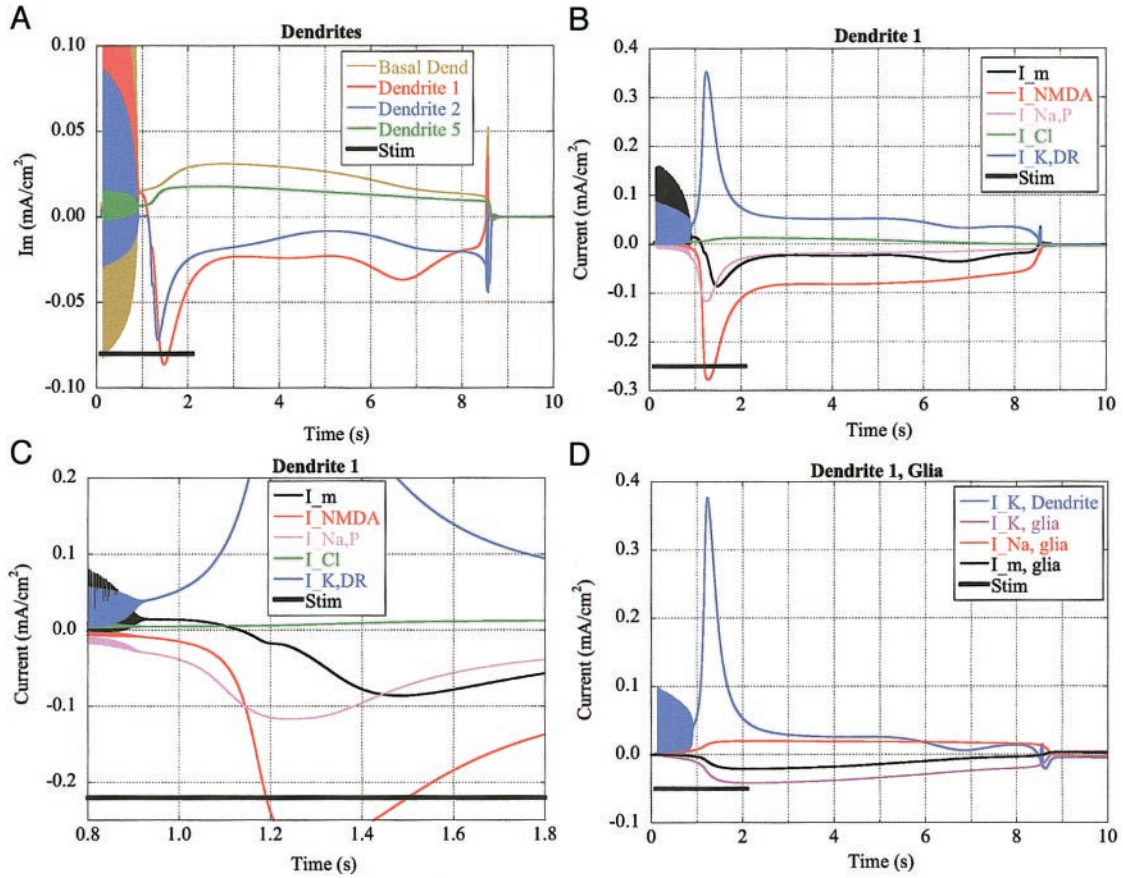

FIG. 4. Membrane currents in dendrites. All four panels from the same simulation. *A*: net membrane currents in 1st, 2nd, and 5th apical dendritic segment and in the basal dendrite. *B*: component ion currents in the 1st apical dendritic segment. *I*_m: net membrane current (also represented in *A*). *I*_NMDA: current controlled by *N*-methyl-D-aspartate (NMDA) receptor. *I*_Na, P: persistent sodium current. *I*_Cl: chloride current. *I*_K, DR: delayed rectifier potassium current. *C*: the currents of *B* shown on expanded scales. *D*: glial "buffer" currents. *I*_K, D1: total potassium current of the neuron's D1 apical dendrite segment ($I_{K,\ DR} - I_{K,\ pump}$. Note that in *B*, only $I_{K,\ DR}$ is represented). *I* K, glia: potassium current through the glial membrane. *I* Na, glia: sodium current through the glial membrane. *I* m, glia: net membrane current through the glial membrane. The stimulus was 0.3 nA for 2 s.

of stimulus raised the intensity requirement and shortened SD duration, and with very short stimuli, SD could not be triggered (Fig. 7). By contrast, the threshold for action potential firing barely changed in the range of 50- to 2,000-ms stimuli, demonstrating that with pulses longer than 50-ms impulse threshold was near "rheobase." The time domain of the strength-duration curves for SD ignition appears to be about two orders of magnitude longer than for action potential firing.

The effects of varying the glia-endothelial "buffer" function on the action potential threshold, SD ignition, and SD duration are illustrated in Fig. 8*A*. To keep the glial resting potential stable, whenever the glial leak conductances were changed, the glial ion pump's carrying capacity had to be adjusted as well. Both glial leak and pump currents moved K^+ from interstitial fluid into the glia-endothelial compartment, both fluxes contributing to buffering $[K^+]_o$. When the glial leak conductances and pump current were small, the threshold for action potential firing was near the SD; in other words the slightest excitation of the neuron lead to SD. When the efficiency of "buffering" excess $[K^+]_o$ was augmented by increasing the glial buffering, the SD ignition level was raised while the firing threshold was minimally affected. With the glial leak 15 times the (arbitrary) baseline, SD could no longer be triggered. The duration of the SD-like depolarization became shorter with each step of increasing glial leak (Fig. 8*A*). The size of the glial compartment set the limit of the capacity of the buffer, and SD duration and its ignition point were also influenced by adjustments of this volume (Fig. 8*B*). When the glial volume was equal to that of the neuron (glial volume 1), SD lasted almost three times longer than when the glia was five times larger than the neuron. Increasing glial size raised the SD ignition point, but beyond volume 5 there was little effect on SD duration or ignition (Fig. 8*B*).

Figure 9 illustrates the effects of changing the specific conductances, g_{NMDA} and $g_{Na,P}$ on the maximal surges of the currents they control (I_{NMDA} and $I_{Na,P}$), on the onset time of SD and on the maximal levels of depolarization (ΔV_m) and $[K^+]_o$ reached during SD. As expected, each current varied in proportion to its controlling conductance. SD onset time advanced as the conductances increased. The effect of $g_{Na,P}$ on SD onset time was more marked than that of g_{NMDA}, probably because $I_{Na,P}$ was activated earlier than I_{NMDA}, even though eventually I_{NMDA} grew to a larger maximal amplitude than did $I_{Na,P}$ (Fig. 4, *B* and *C*). Varying the conductance g_{NMDA} or $g_{Na,P}$ had, however, little effect on the final level of depolarization or of the maximum of $[K^+]_o$ (Fig. 9).

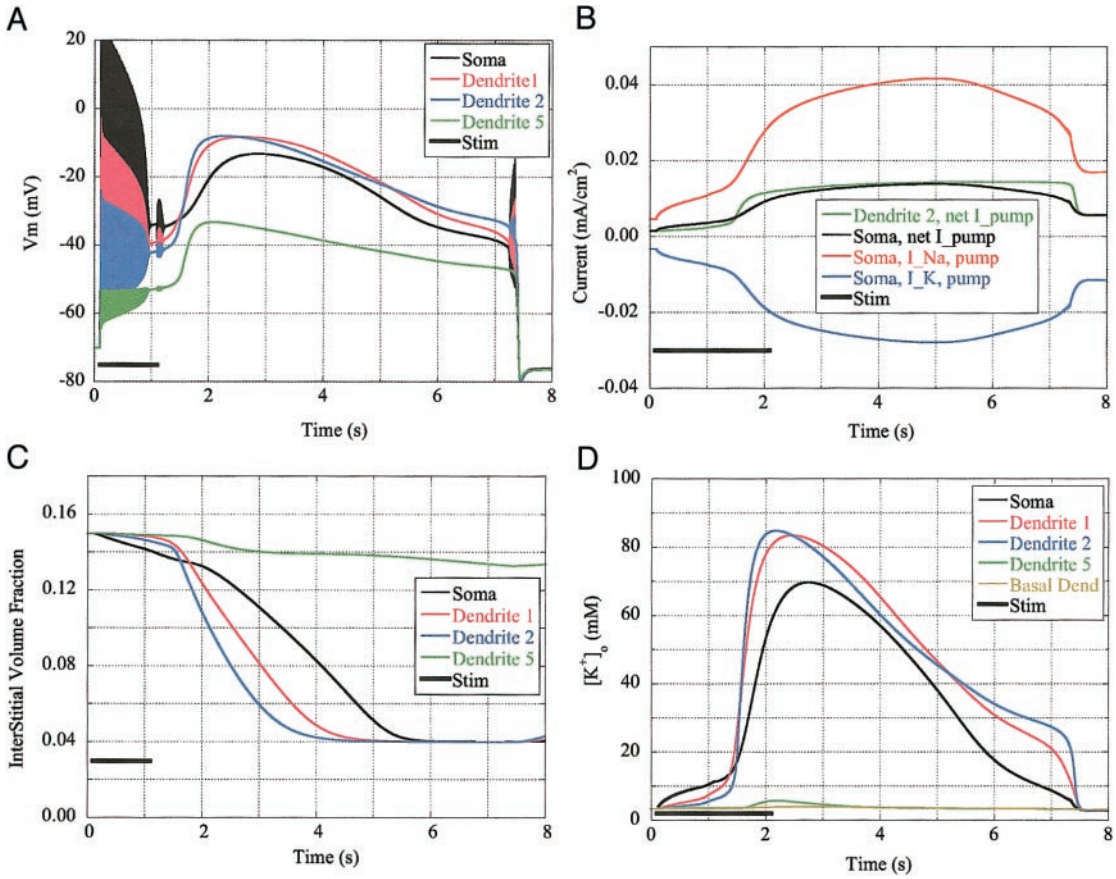

FIG. 5. The course of variables in soma and dendrites compared. Data from the same simulation as Fig. 4. *A*: membrane potential changes in the neuron soma, 1st, 2nd, and 5th apical dendritic segments. *B*: currents generated by the 3Na-2K ion pumps. Dendrite 2, *I*_pump: net pump current in the second apical dendritic segment. Soma, *I*_pump: net pump current of the soma membrane. Soma, *I*_Na, pump: Sodium current generated by the ion pump in the soma membrane. Soma, *I*_K, pump: Potassium current generated by the ion pump in the soma membrane. *C*: interstitial volume fraction (ISVF) at the neuron soma and the 1st, 2nd, and 5th apical dendritic segments. ISVF is expressed as fraction of neuron volume at each segment. *D*: potassium concentration in interstitial space of the neuron soma, the 1st, 2nd, and 5th apical dendrite segment and the basal dendrite. Note that during stimulation the responses are greatest in the soma, but at SD onset dendrite 1 followed by dendrite 2 take the lead, while dendrite 5 and basal dendrite remain "passive".

The "window" current of $I_{Na,T}$ could be changed by shifting the voltages of either the activation of $g_{Na,T}$ (Hodgkin and Huxley's "*m*" parameter) or of its steady-state inactivation [h_∞] (Hodgkin and Huxley 1952). Shifting the midpoint of the activation function, m^3, by −5 mV, from −23.5 to −28.5 mV decreased as expected the firing threshold. It also lowered the ignition point of SD from 0.3 to 0.19 nA (pulse duration, 500 ms) and increased SD duration from 14.4 to 15.3 s. A further shift by −5 mV caused the model to become unstable, generating recurrent "spontaneous" SD episodes.

SD in the complete cell model

The data presented so far were all produced in the simplified model cell. To validate these results, a smaller number of simulations were performed using the more realistic complete cell (see METHODS). The main features of the more complex computations were quite similar, but quantitative aspects became more life-like. Most markedly, the complete cell generated SDs of longer duration than did the simplified cell. Figure 10 illustrates such a trial. Figure 10, *A* and *B*, shows membrane voltage and the equilibrium potentials of dendritic segment 2 on two different time scales and *C* and *D* the corresponding currents. As in the simplified cell, the SD-like depolarization was driven by sustained inward current in apical dendrites. Activation of $I_{Na,P}$ initiated the process but I_{NMDA} then took over as the main driver. Also similarly to the simplified cell, SD was always initiated and governed by dendritic currents, with the soma following the dendritic lead (not illustrated).

Hypoxic SD-like depolarization (HSD)

To simulate anoxia or other energy failure, we set the 3Na/2K ion pump to zero. Because in ischemia capillary circulation stops, the capacity of the glial compartment was set to be equal to the volume of the neuron (see DISCUSSION). The ion pump of the glia remained active, as it may be assumed that glycolitic metabolism continues to produce ATP in glial cells for many minutes even during anoxia. As expected, in this condition ions flowed unopposed through the leak channels of the neuron membrane, $[K^+]_o$ slowly increased and the membrane depolarized without external stimulation (Fig. 11). When V_m reached threshold, a burst of action potentials occurred, until the depolarization inactivated $I_{Na,T}$ and silenced the firing. Shortly thereafter I_m in the active segments of the apical dendrites turned inward (Fig. 11*D*) causing SD-like depolar-

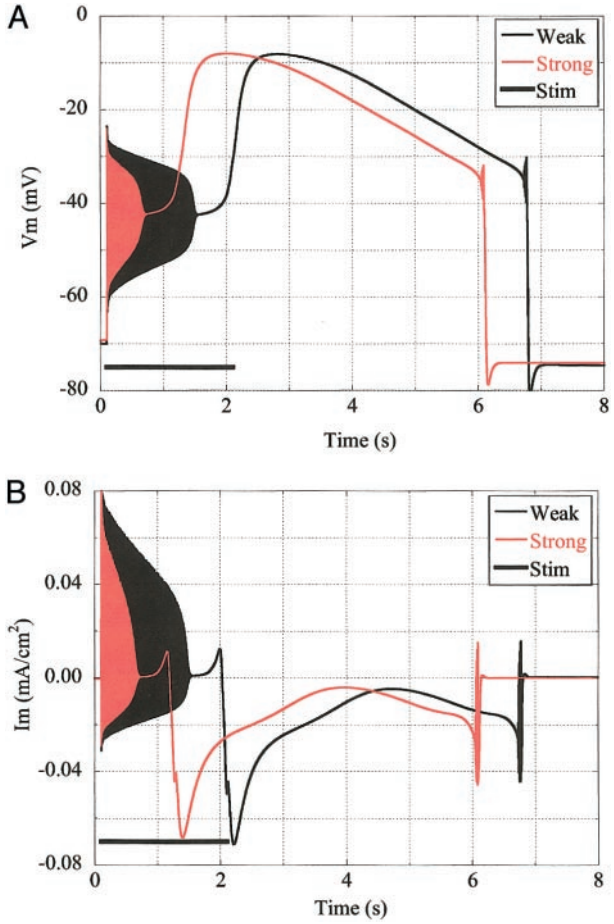

FIG. 6. The course of SD is independent of stimulus intensity. All traces from the 2nd dendritic segment. Weak stimulus: 0.385 nA for 2 s. Strong stimulus: 0.45 nA for 2 s. *A*: membrane potential. *B*: net membrane current.

ization. At the time of onset of HSD, we turned on the ion pump in the neuron, imitating reoxygenation of a hypoxic tissue slice. Reinstating active ion transport did not immediately start recovery. Only after SD ran its typical course was it

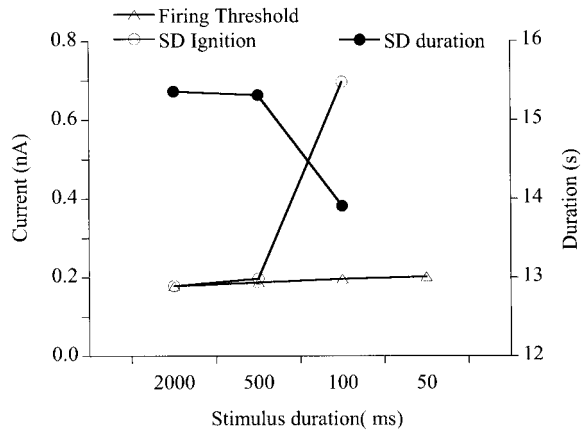

FIG. 7. The effect of varying stimulus duration on the threshold of firing action potentials, SD ignition point, and SD duration. The left ordinate shows stimulus intensities in nA, the right ordinate SD duration in seconds. The membrane parameters were constant for the 4 sets of data. SD duration was measured from the moment of inward turn of the net current of D2 apical dendrite segment to the half-repolarization of V_m.

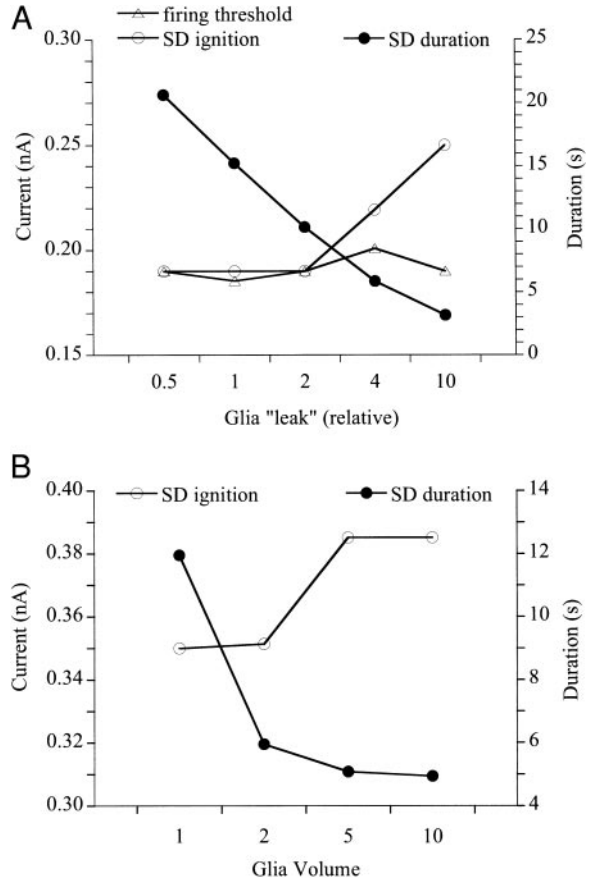

FIG. 8. The effect of changing glial parameters on SD ignition point, SD duration, and action potential threshold. *A*: varying glial membrane conductances and glial pump current. Glial $g_{Na,\ leak}$ $g_{K,\ leak}$, $g_{Cl,\ leak}$, and pump currents were adjusted in equal proportion in all segments of the model. Neuron membrane parameters were not changed. Left ordinate scale: SD duration (s). Right ordinate scale: stimulus current (nA). The stimulus duration was 2 s for all trials. *B*: varying glial volume, expressed relative to neuron volume (1 means glia = neuron). Stimulus duration 1 s. Neuron parameters constant.

followed by "posthypoxic" hyperpolarization and eventual return to resting conditions.

In another simulation, the pump remained at zero even after SD-like depolarization, with other initial conditions the same as for Fig. 11. HSD set in similarly to Fig. 11, but then instead of recovering, ion concentrations and V_m subsided toward a level representing Donnan-equilibrium. This final state may be compared with "terminal depolarization" of live brain. In yet another trial, both the neuronal and the glial ion pump were set to zero. As a result $[K^+]_o$ accumulated very rapidly and HSD set in about 50 ms and depolarization reached a plateau in 0.5 s. During the HSD V_m transiently depolarized to about −6 mV, then V_m, E_K, E_{Na}, and E_{Cl} slowly converged toward equilibrium around −28 mV.

When the maximal conductances of the NMDA channel and the persistent Na channel were set to low levels, then even if the ion pump was inactive, no SD-like depolarization occurred. The burst of impulses was triggered and then inactivated as in Fig. 11, but then V_m and ion concentrations slowly and gradually approached the Donnan-like state. In this case, the membrane current never turned inward in the apical dendrites and the slow depolarization was governed by the shift in ion concentrations.

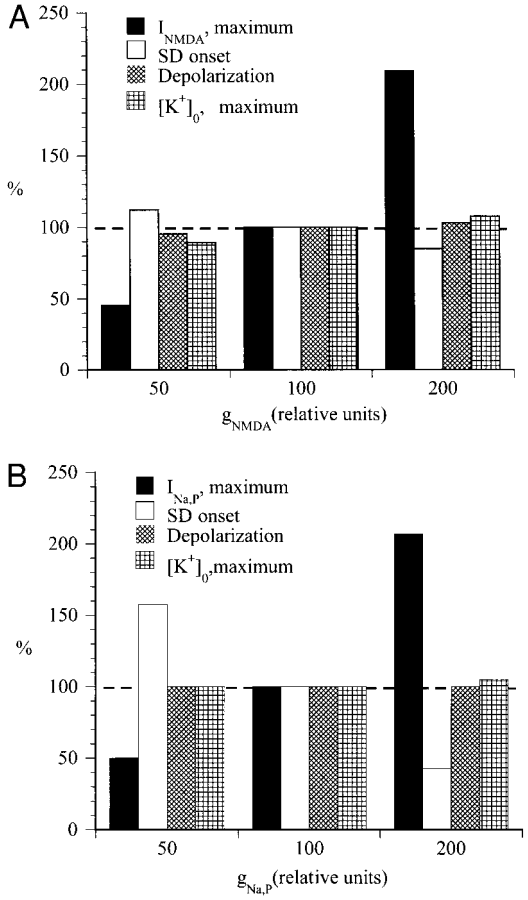

FIG. 9. The effect of changing neuron ion conductances. *A*: changing the maximal conductances of the NMDA-controlled channel (g_{NMDA}) with other parameters constant. All values in relative units. *I*_NMDA, maximum: the amplitude of the maximal surge of the NMDA-controlled current during SD. 100% = −0.32 mA/cm^2. SD onset: the time from the start of stimulation until the inward turning of the net membrane current in D2 apical segment (100% = 496 ms). Depolarization: the change of V_m from the "rest" state (100% = from −69 to −4.3 mV in the D2 segment). $[K^+]_o$, maximum: the maximal level of interstitial potassium concentration during SD at the D2 segment (100% = 99.8 mM) *B*: the effect of changing the maximal persistent sodium conductance ($g_{Na,P}$). *I*_Na, P: maximal amplitude of the persistent sodium current (100% = −0.12 mA/cm^2). Stimulus duration for all entries 500 ms.

DISCUSSION

Four conclusions emerge. Three confirm what has previously been suspected: that SD is an all-or-none process; that rising $[K^+]_o$ and/or overflow of glutamate can initiate SD; and that ion channels normally present in neuron membranes can mediate the SD-like depolarization. The fourth insight is novel: namely that the critical condition for SD ignition is the activation of net persistent inward membrane ion current in apical dendrites.

Accelerating, regenerative, all-or-none type depolarization invariably ensued whenever the net dendritic membrane current turned inward. This condition is analogous to the well-known threshold of action potentials, which is reached when the inward sodium current, I_{Na} exceeds the outward potassium current, I_K (Hodgkin and Huxley 1952; Katz 1966). Accordingly, in the pyramidal neurons modeled here, impulses were generated in the neuron soma when $I_{Na,T}$ exceeded $I_{K,A} + I_{K,DR}$. By contrast, SD did not arise in the soma but in an apical dendritic segment, and it depended on shifting the balance so as to favor slowly inactivating (persistent) inward over outward currents. The SD ignition condition may be formalized as follows

$$(I_{Na,P} + I_{NMDA} + I_{Na,leak}) > (I_{K,DR} + I_{Na,Kpump} + I_{Cl} + I_{K,leak})$$

The simulations demonstrated the independence of the SD process from the strength of the triggering stimulus, confirming its all-or-none character. A fixed threshold in a single variable could, however, not be defined for the triggering of SD. Rather, there had to be a confluence of several factors, reminiscent of the Reynolds number for turbulent flow. Especially both V_m and $[K^+]_o$ had to shift appropriately to achieve sufficient activation of $I_{Na,P}$ and/or I_{NMDA}. It is for this reason that we prefer the expression "ignition point" over "threshold" to describe SD initiation. Varying $g_{Na,P}$ or g_{NMDA} influenced the stimulus required to trigger SD and the onset time of SD but did not affect the final level of the depolarization nor of the $\Delta[K^+]_o$. If one of the persistent conductances was insufficient, the onset of SD was delayed, but the deficit was eventually compensated by the remaining conductance. This agrees with our earlier conclusion based on data from both live tissue and computer simulation that the final level of depolarization is governed by feedback and not by the number of channels available to open (Kager et al. 2000; Müller and Somjen 2000b).

The simulations confirm the long-suspected roles of both, failing regulation of K^+ ions as well as of the overflow of glutamate in the generation of SD (Billups et al. 1998; Grafstein 1956; van Harreveld 1978; van Harreveld and Fifková 1970). Unbridled rise of $[K^+]_o$ can result either from the excessive outpouring of K^+ from cells or from defective regulation, for example, due to the inhibition of the 3Na/2K ion pump (Balestrino et al. 1999). Similarly, glutamate could overflow into interstitial fluid rise either because of its excessive release or failure of its re-uptake (Billups et al. 1998). There is thus justification of Van Harreveld's dual hypothesis, which assigns equal roles to K^+ and to glutamate (van Harreveld 1978).

Neither SD nor HSD requires working synapses; both can occur in the presence of TTX, and in the absence of external Ca^{2+} (reviewed in Somjen 2001). Because blocking glutamatergic synapses does delay SD and HSD even if it does not abolish them, it is assumed that overflow of glutamate released from depolarizing neurons, axon endings, and astrocytes does cooperate in igniting SD. Our assigning NMDA currents to the apical dendritic segments 1–3 was somewhat arbitrary. In brain cells in situ, the variations of the distribution and overall density of various types of synaptic and extrasynaptic glutamate receptors probably influences the inclination for SD-like depolarization.

In experiments on intact brain tissue, SD can be provoked, among others, by DC current, the local application of a high-K^+ solution, stabbing or tapping the exposed brain, or high-intensity, high-frequency repetitive electrical stimulation. Each of these interventions induces profound sustained depolarization of neurons; this is represented by the depolarizing stimulating current used in our trials.

SD was not ignited in all dendritic segments at once. It usually started in the segment near to the soma and was conducted from there centrifugally into the distal dendritic tree and centripetally into the soma (see also Kager et al. 2000).

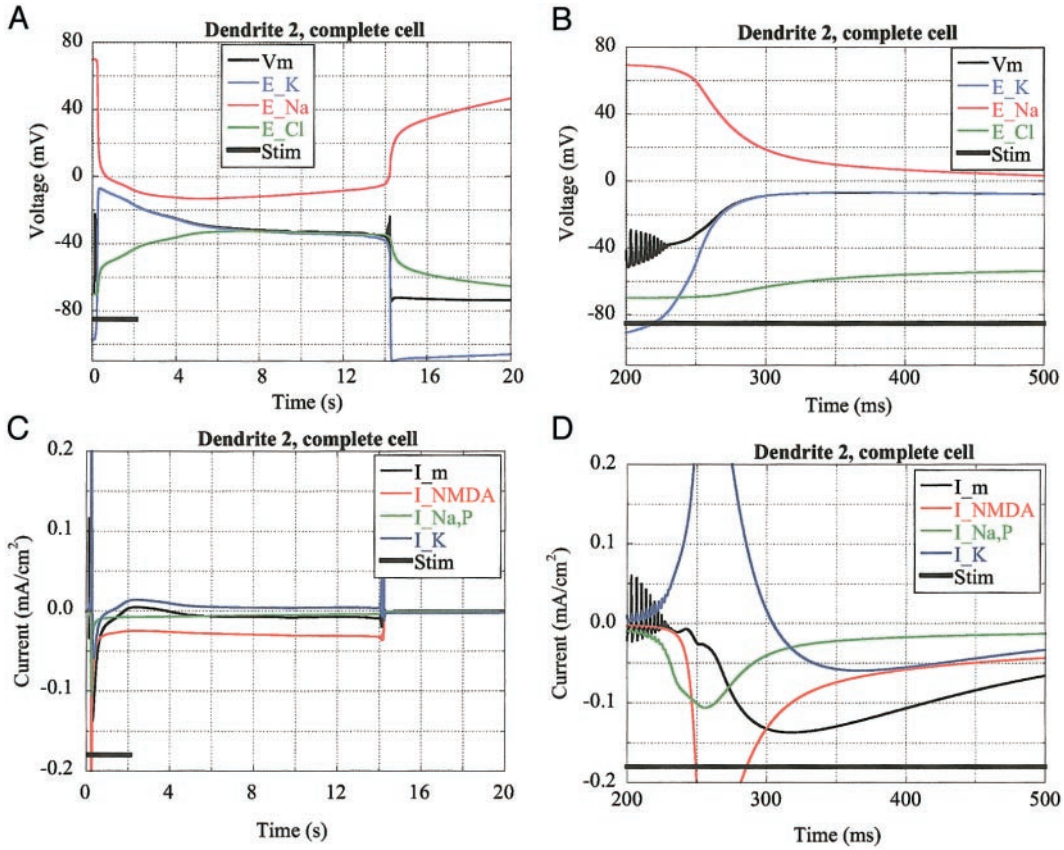

FIG. 10. SD in the "complete" neuron model. All 4 panels are from the same simulation. *A* and *B*: membrane potential and ion equilibrium potentials in the 2nd apical dendritic segment on two different time scales. *C* and *D* membrane currents on different time scales. Symbols as in Fig. 1.

The onset of SD ignition depended mainly on the rate of increase in $[K^+]_o$. The outflow of K^+ is governed by depolarization, which in turn depends on channel density and rate of activation of the channels. Channel density, which was represented as maximal conductance (*g*), was uniform along the model's apical dendritic membrane, except the passive outermost segments. The rate of activation of the channels depended on the initial depolarization, which was fastest in the dendritic segments adjacent to the soma. The extracellular accumulation and intracellular depletion of K^+ were, however, also influenced by the surface-to-volume ratio, which increased with distance from the soma as dendrites tapered. Because of the greater surface-to-volume ratio, the rate of rise of $[K^+]_o$ at the D2 segment overtook that at D1, and it also reached a higher summit around D2 than D1 (Fig. 5*D*). In hippocampus in situ, SD consistently begins in the region of apical dendrites before it erupts in the layers containing pyramidal cell somata (Herreras and Somjen 1993a,b). Conduction along dendrites is much faster than SD propagation among cells.

In the model, the 3Na/2K membrane ion pump regulated the distribution of ions, assisted by the glial "compartment" which buffered both the rise of $[K^+]_o$ and the decline of $[Na^+]_o$ in the interstitial space. The buffering function was insufficient, if either the volume of the glial compartment was too small to accommodate the overflow, or if the glial membrane leak and pump functions were too low. In brain tissue in situ astrocytes and capillary endothelium probably act in concert in limiting the rise of $[K^+]_o$. Astrocyte processes are believed to siphon K^+ ions into the pericapillary space (Newman 1986, 1995), from where the transporters of the endothelial cell membranes can move them into circulating blood (Bradbury 1979; Cserr 1965; Somjen 2002). Siphoning into circulating blood can make the effective capacity of the buffer in intact living brains essentially infinite. Therefore as long as blood flows in brain, the efficiency of the buffer depends entirely on the rates of transport across the glial and endothelial membranes and along the glial processes. When $[K^+]_o$ drops at the end of excessive excitation of neurons, the buffering process must be reversed and lost K^+ must return to the neurons by reverse flux through the glia-endothelial system. In ischemia, however, circulating blood is not available to receive excess load of K^+ from the glial cytosol, and buffering becomes limited by the size of the glial compartment itself. In the simulation of ischemia (Fig. 11), we set the glial buffer capacity equal to the neuron volume on the basis of work by Kuffler and Nicholls (1966), who estimated that glial cells occupy about half the volume of cerebral tissue. In hippocampus the glial compartment is, however, probably much smaller than in neocortex (Green 1964).

The size of the interstitial space is important because it determines the dynamics of extracellular concentration when K^+ is released from neurons. We chose the ISVF to conform to values reported for rodent hippocampus (McBain et al. 1990). When we made the simulated ISVF larger, SD became less likely, but we did not explore its effect in detail.

The rise of $[K^+]_o$ can promote regenerative depolarization in more than one way. Excess $[K^+]_o$ depolarizes neurons as well

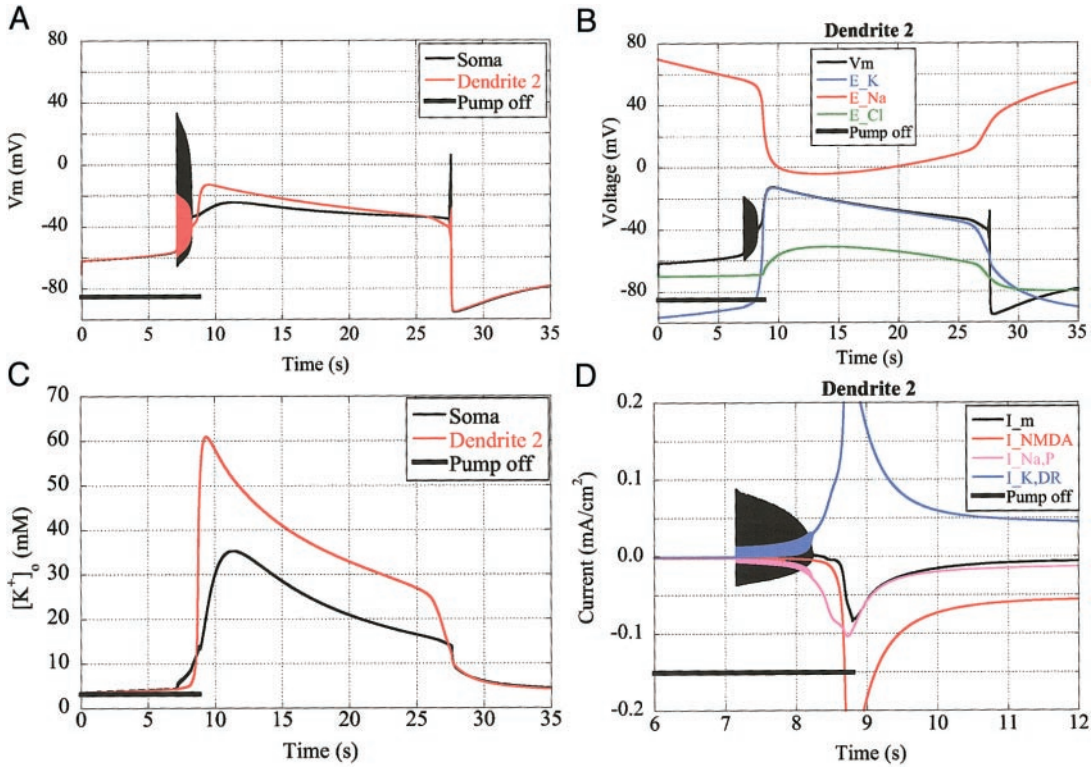

FIG. 11. Simulated hypoxic SD-like depolarization (HSD). All 4 panels from the same simulation. "Pump off": the 3Na/2K ion pump of the neuron was set to 0. Other symbols as in Fig. 1, 4, and 5. *A*: membrane voltage in the neuron soma and in the 2nd apical dendritic segment.. *B*: membrane potential and ion equilibrium potentials in the 2nd apical dendritic segment. *C*: extracellular potassium concentration outside the neuron soma and the 2nd apical dendrite segment. *D*: expanded view of membrane currents during the onset of HSD in the 2nd dendrite segment.

as glial cells. As long as depolarization remains below the level of inactivation, it enhances neuron excitability. It also causes the release of transmitters, of which glutamate is the most relevant for SD, at least in hippocampus and neocortex. High $[K^+]_o$ can promote the overflow of glutamate in at least three ways: by depolarization of presynaptic terminals thereby activating calcium inflow and initiating transmitter release from synaptic vesicles; by the reversal of the glutamate transporter of glial cells (Billups et al. 1998); and by K^+-induced swelling of glia (Basarsky et al. 1999). In addition, high $[K^+]_o$ enhances NMDA receptor activation (Poolos and Kocsis 1990) and also potentiates the persistent Na^+ current, $I_{Na,P}$ (Somjen and Müller 2000).

Setting the 3Na/2K ion pump in the neuron to zero simulated hypoxia as seen in hippocampal tissue slices (Müller and Somjen 2000a,b). As in live brain tissue, during simulated energy failure $[K^+]_o$ began to rise due to the unopposed leak current. V_m shifted abruptly by a few millivolts due to the cessation of the electrogenic pump current and then depolarized slowly until firing threshold was reached, triggering a burst of rapidly inactivating action potentials. Shortly thereafter SD-like depolarization was initiated when I_m in the active apical dendrite segments turned inward. The sequence of events during the simulated hypoxic SD in Fig. 11 resembled the SD episodes illustrated in the preceding figures. Reoxygenation, simulated by activating the ion pump, permitted eventual recovery to the resting state, but only after SD ran its full course, as it happens also in live brain tissue. In simulated terminal anoxia, with the pump remaining at zero for the entire simulation, membrane voltage and ion levels settled toward a Donnan equilibrium. The equilibrium depended on the presence of impermeant anions in the cytosol and on the limit to cell swelling set by the minimum to which the interstitial space was allowed to shrink. In real tissues, dying cells eventually release their content of organic anions so that membrane potentials and ion gradients terminate at zero.

The cell model used for most of these trials was morphologically simpler than the complete cell modeled after a reconstructed hippocampal neuron (Cannon et al. 1998; Kager et al. 2000). The behavior of the two models differed in quantitative details, but it was qualitatively similar. The complete cell had a much wider expanse of dendritic surface. To make input resistances comparable (in most trials 50–90 MΩ for the simplified cell, 56 MΩ for the complete cell), the leak conductance had to be set higher per unit surface area for the simple cell. Whenever leak was changed, the pump capacity had to be adjusted as well to maintain stability at "rest." As may be expected, increasing leak also increased the stimulus intensity required for triggering action potentials or to ignite SD.

The model did not incorporate all the ion channels and transporters known to exist in live central brain cells. Most notable is the absence of calcium ions and calcium channels. It is, however, well known that SD and HSD can readily occur in brain slices in the absence of Ca^{2+} in the bathing fluid (Somjen 2001). Without Ca^{2+}, neither Ca-dependent K currents nor the Ca/Na exchanger could be simulated. Without Ca-dependent K currents, there was no "slow" hyperpolarizing afterpotential, and the rate of firing of action potentials was higher than is

usual in vivo. These deficiencies affect firing patterns but not the essential features of SD-like response.

The trajectories of voltages and ion concentrations during simulated SD episodes were similar to SD seen in neurons and glial cells of live brains with one notable difference. The membrane potential repolarized at the end of SD more abruptly than in recordings from live cells. This could be because of the restricted possibility of ion diffusion since the model was of a single neuron not of tissue with many cells and an interconnected labyrinth of interstitial spaces. Another limitation of this model was the assumption of zero voltage throughout the interstitial space. A more perfect version should include computation of extracellular current flow, voltage gradients, and electro-diffusion. Working with just one cell also prevented simulation of the propagation of an SD wave. Other models were aimed at solving SD propagation (reviewed in Grafstein 1963; Nicholson 1993; Shapiro 2001; Somjen 2001). An ultimate model should combine the two approaches.

REFERENCES

AITKEN PG, BORGDORFF AJ, JUTA AJA, KIEHART DP, SOMJEN GG, AND WADMAN WJ. Volume changes induced by osmotic stress in freshly isolated rat hippocampal neurons. *Eur J Physiol* 436: 991–998, 1998.

BALESTRINO M, YOUNG J, AND AITKEN PG. Block of (Na^+,K^+)ATPase with ouabain induced spreading depression-like depolarization in hippocampal slices. *Brain Res* 838: 37–44, 1999.

BASARSKY TA, FEIGHAN D, AND MACVICAR BA. Glutamate release through volume-activated channels during spreading depression. *J Neurosci* 19: 6439–6445, 1999.

BILLUPS B, ROSSI D, OSHIMA T, WARR O, TAKAHASHI M, SARANTIS M, SZATKOWSKI M, AND ATTWELL D. Physiological and pathological operation of glutamate transporters. *Prog Brain Res* 116: 45–57, 1998.

BRADBURY MWB. *The Concept of the Blood-Brain Barrier*. Chichester, UK: Wiley, 1979.

BUREŠ J, BUREŠOVÁ O, AND KRIVÁNEK J. The mechanism and applications of Leao's spreading depression of electroencephalographic activity. *Prague, Academia* 1974.

CANNON RC, TURNER DA, PYAPALI GK, AND WHEAL HV. An on-line archive of reconstructed hippocamnpal neurons. *J Neurosci Methods* 84: 49–54, 1998.

CSERR H. Potassium exchange between cerebrospinal fluid, plasma, and brain. *Am J Physiol* 209: 1219–1226, 1965.

GARCÍA RAMOS J AND DE LA CERDA E. On the ionic nature of the slow potential and impedance changes of spreading depression. *Acta Physiol Latinoam* 24: 216–227, 1974.

GRAFSTEIN B. Mechanism of spreading cortical depression. *J Neurophysiol* 19: 154–171, 1956.

GRAFSTEIN B. Neuronal release of potassium during spreading depression. In: *Brain Function. Cortical Excitability and Steady Potentials*, edited by MAB Brazier Berkeley, CA: University of California, 1963, p. 87–124.

GREEN JD. The hippocampus. *Physiol Rev* 44: 561–608, 1964.

HERRERAS O AND SOMJEN GG. Analysis of potential shifts associated with recurrent spreading depression and prolonged unstable SD induced by microdialysis of elevated K^+ in hippocampus of anesthetized rats. *Brain Res* 610: 283–294, 1993a.

HERRERAS O AND SOMJEN GG. Propagation of spreading depression among dendrites and somata of the same cell population. *Brain Res* 610: 276–282, 1993b.

HINES M AND CARNEVALE NT. The NEURON simulation environment. *Neural Computat* 9: 1179–1209, 1997.

HODGKIN AL AND HUXLEY AF. A quantitative description of membrane current and its application to conduction and excitation in nerve. *J Physiol (Lond)* 117: 500–544, 1952.

JING J, AITKEN PG, AND SOMJEN GG. Interstitial volume changes during spreading depression (SD) and SD-like hypoxic depolarization in hippocampal tissue slices. *J Neurophysiol* 71: 2548–2551, 1994.

KAGER H, WADMAN WJ, AND SOMJEN GG. Simulated seizures and spreading depression in a neuron model incorporating interstitial space and ion concentrations. *J Neurophysiol* 84: 495–512, 2000.

KAGER H, WADMAN WJ, AND SOMJEN GG. Simulation of membrane current and ion concentrations in a neuron predicts epileptiform discharge and spreading depression (SD). *Soc Neurosci Abstr* 27: 559.3, 2001.

KATZ B. *Nerve, Muscle and Synapse*. New York: McGraw-Hill 1966.

KETELAARS SOM, GORTER JA, VAN VLIET EA, LOPES DA SILVA FH, AND WADMAN WJ. Sodium currents in isolated rat CA1 pyramidal and dentate granule neurons in the post-status epilepticus model of epilepsy. *Neuroscience* 105: 109–120, 2001.

KUFFLER SW AND NICHOLLS JG. The physiology of neuroglial cells. *Erg Physiol* 57: 1–90, 1966.

LEÃO AAP. Spreading depression of activity in the cerebral cortex. *J Neurophysiol* 7: 359–390, 1944.

MAGEE JC AND JOHNSTON D. Characterization of single voltage-gated Na^+ and Ca^{2+} channels in apical dendrites of rat CA1 pyramidal neurons. *J Physiol (Lond)* 487: 67–90, 1995.

MCBAIN CJ, TRAYNELIS, SF AND DINGLEDEINE R. Regional variation of extracellular space in hippocampus under physiological and pathological conditions. *Science* 249: 674–677, 1990.

MÜLLER M AND SOMJEN GG. Inhibition of major cationic inward currents prevents spreading depression-like hypoxic depolarization in rat hippocampal tissue slices. *Brain Res* 812: 1–13, 1998.

MÜLLER M AND SOMJEN GG. Na^+ and K^+ concentrations, extra- and intracellular voltages and the effect of TTX in hypoxic rat hippocampal slices. *J Neurophysiol* 83: 735–745, 2000a.

MÜLLER M AND SOMJEN GG. Na^+ dependence and the role of glutamate receptors and Na^+ channels in ion fluxes during hypoxia of rat hippocampal slices. *J Neurophysiol* 84: 1869–1880, 2000b.

NEWMAN EA. High potassium conductance in astrocyte endfeet. *Science* 233: 453–454, 1986.

NEWMAN EA. Glial cell regulation of extracellular potassium. In: *Neuroglia*, edited by Kettenman H and Ransom BR. New York: Oxford, 1995, p. 717–731.

NICHOLSON C. Volume transmission and the propagation of spreading depression. In: *Migraine: Basic Mechanisms and Treatment*, edited by Lehmenkühler A, Grotemeyer KH, and Tegtmeier F. München: Urban and Schwarzenberg, 1993, p. 293–308.

POOLOS NP AND KOCSIS JD. Elevated extracellular potassium concentration enhances synaptic activation of *N*-mtheyl-D-aspartate receptors in hippocampus. *Brain Res* 508: 7–12, 1990.

SHAPIRO BE. Osmotic forces and gap junctions in spreading depression: a computational model. *J Computat Neurosci* 10: 99–120, 2001.

SOMJEN GG. Mechanisms of spreading depression and hypoxic SD-like depolarization. *Physiol Rev* 81: 1066–1096, 2001.

SOMJEN GG. Ion regulation in the brain: implications for pathophysiology. *Neuroscientist*: 8: 254–267, 2002.

SOMJEN GG, KAGER H, AND WADMAN WJ. Conditions for triggering simulated spreading depression (SD) (Abstract). *FASEB J* 15: A846, 2001.

SOMJEN GG AND MÜLLER M. Potassium-induced enhancement of persistent inward current in hippocampal neurons in isolation and in tissue slices. *Brain Res* 885: 102–110, 2000.

STEINHÄUSER C, TENNIGKEIT M, MATTHIES H, AND GÜNDEL J. Properties of the fast sodium channels in pyramidal neurons isolated from the CA1 and CA3 areas of the hippocampus of postnatal rats. *Pflügers Arch* 415: 756–761, 1990.

TOBIASZ C AND NICHOLSON C. Tetrodotoxin resistant propagation and extracellular sodium changes during spreading depression in rat cerebellum. *Brain Res* 241: 329–333, 1982.

TRAUB RD, MILES R, AND JEFFERYS JGR. Synaptic and intrinsic conductances shape picrotixin-induced sychronized after-discharges in the guinea pig hippocampal slice. *J Physiol (Lond)* 461: 525–547, 1993.

TRAUB RD, JEFFERYS JGR, MILES R, WHITTINGTON MA, AND TÓTH K. A branching dendritic model of a rodent CA3 pyramidal neurone. *J Physiol (Lond)* 481: 79–95, 1994.

VAN HARREVELD A. Compounds in brain extracts causing spreading depression of cerebral cortical activity and contraction of crustacean muscle. *J Neurochem* 3: 300–315, 1959.

VAN HARREVELD A AND FIFKOVÁ E. Glutamate release from the retina during spreading depression. *J Neurobiol* 2: 13–29, 1970.

VAN HARREVELD A. Two mechanisms for spreading depression in the chicken retina. *J Neurobiol* 9: 419–431, 1978.

WADMAN WJ, JUTA AJA, KAMPHUIS W, AND SOMJEN GG. Current source density of sustained potential shifts associated with electrographic seizures and with spreading depression in rat hippocampus. *Brain Res* 570: 85–91, 1992.